

Supplementary Materials

Guangxia Piao,^a Sun Hee Yoon,^b Hyun Gil Cha,^c Dong Suk Han^{d,*} and Hyunwoong Park^{a,*}

^a School of Energy Engineering, Kyungpook National University, Daegu 41556, Korea

^b Petroleum Engineering Program, Texas A&M University at Qatar, Doha 23874, Qatar

^c Center for Bio-based Chemistry, Korea Research Institute of Chemical Technology, Ulsan 44429, Korea

^d Center for Advanced Materials, Qatar University, Doha 2713, Qatar

*To whom correspondence should be addressed:

(D.S. Han) dhan@qu.edu.qa; Tel: +974-4403-5686

(H. Park) hwp@knu.ac.kr; Tel: +82-53-950-8973

Table S1. Adsorption energies of HMF and bond lengths of aldehyde and alcohol groups for adsorbed HMF on Bi, Sn, and BiSn.

	Adsorption Energy (eV)	Bond length Aldehyde C=O	Bond length Alcohol C-O
Free HMF		1.225	1.439
Adsorbed HMF			
Bi(012)	-2.58	1.207	1.444
BiSn	-1.24	1.226	1.446
Sn(101)	-0.93	1.16	1.438

Table S2. Catalytic activities on different electrodes for electrochemical hydrogenation of HMF to BHMF

No.	Material	Electrolyte	E_{on} (V)	J ($mA\ cm^{-2}$)	FE_{BHMF}	Ref.
1	Ag/Cu foil	0.5 M Borate buffer (pH 9.2, 20 mM HMF)	-0.2	-6.9	99%	1
2	Ag/Cu foam	0.5 M Borate buffer (pH 9.2, 50 mM HMF)	-0.18	-16	83%	2
3	Ag NP/C	0.5 M Borate buffer (pH 9.2, 20 mM HMF)	-0.31	-6.8	96.2%	3
4	Ag foil	0.5 M Borate buffer (pH 9.2, 20 mM HMF)	-0.3	-3.2	75.8%	4
5	In foil	0.5 M Borate buffer (pH 9.2, 20 mM HMF)	-0.4	-2.9	98.8%	4
6	Cd foil	0.5 M Borate buffer (pH 9.2, 20 mM HMF)	-0.35	-3.2	94.5%	4
7	Fe foil	0.5 M Borate buffer (pH 9.2, 20 mM HMF)	-0.2	-6.2	72.8%	4
8	Cu foil	0.5 M Borate buffer (pH 9.2, 20 mM HMF)	-0.38	-3.5	55.6%	4
9	Ti foil	0.5 M Borate buffer (pH 9.2, 20 mM HMF)	-0.6	-2	6.9%	4
10	Co foil	0.5 M Borate buffer (pH 9.2, 20 mM HMF)	-0.25	-2.5	28.9%	4
11	W foil	0.5 M Borate buffer (pH 9.2, 20 mM HMF)	-0.4	-4.5	12.4%	4
12	Ni foil	0.5 M Borate buffer (pH 9.2, 20 mM HMF)	-0.22	-2.5	42.6%	4
13	BDD	0.1 M carbonate buffer (10 mM HMF)	-0.55	-0.85	18%	5
14	Glassy carbon	0.1 M carbonate buffer (10 mM HMF)	-0.45	-1.0	30%	5

Reference information in Figure 8 and Table S2

- (1) Roylance, J. J.; Kim, T. W.; Choi, K.-S. Efficient and Selective Electrochemical and Photoelectrochemical Reduction of 5-Hydroxymethylfurfural to 2,5-Bis(hydroxymethyl)furan using Water as the Hydrogen Source. *ACS Catal.* **2016**, *6* (3), 1840-1847.
- (2) Sanghez de Luna, G.; Ho, P. H.; Sacco, A.; Hernandez, S.; Velasco-Velez, J. J.; Ospitali, F.; Paglianti, A.; Albonetti, S.; Fornasari, G.; Benito, P. AgCu Bimetallic Electrocatalysts for the Reduction of Biomass-Derived Compounds. *ACS Appl. Mater. Interfaces* **2021**, *13* (20), 23675-23688.
- (3) Chadderdon, X. H.; Chadderdon, D. J.; Pfennig, T.; Shanks, B. H.; Li, W. Paired electrocatalytic hydrogenation and oxidation of 5-(hydroxymethyl)furfural for efficient production of biomass-derived monomers. *Green Chem.* **2019**, *21* (22), 6210-6219.
- (4) Lee, D. K.; Kubota, S. R.; Janes, A. N.; Bender, M. T.; Woo, J.; Schmidt, J. R.; Choi, K. S. The Impact of 5-Hydroxymethylfurfural (HMF)-Metal Interactions on the Electrochemical Reduction Pathways of HMF on Various Metal Electrodes. *ChemSusChem* **2021**, *14* (20), 4563-4572.
- (5) Kloth, R.; Vasilyev, D. V.; Mayrhofer, K. J. J.; Katsounaros, I. Electroreductive 5-Hydroxymethylfurfural Dimerization on Carbon Electrodes. *ChemSusChem* **2021**, *14* (23), 5245-5253.

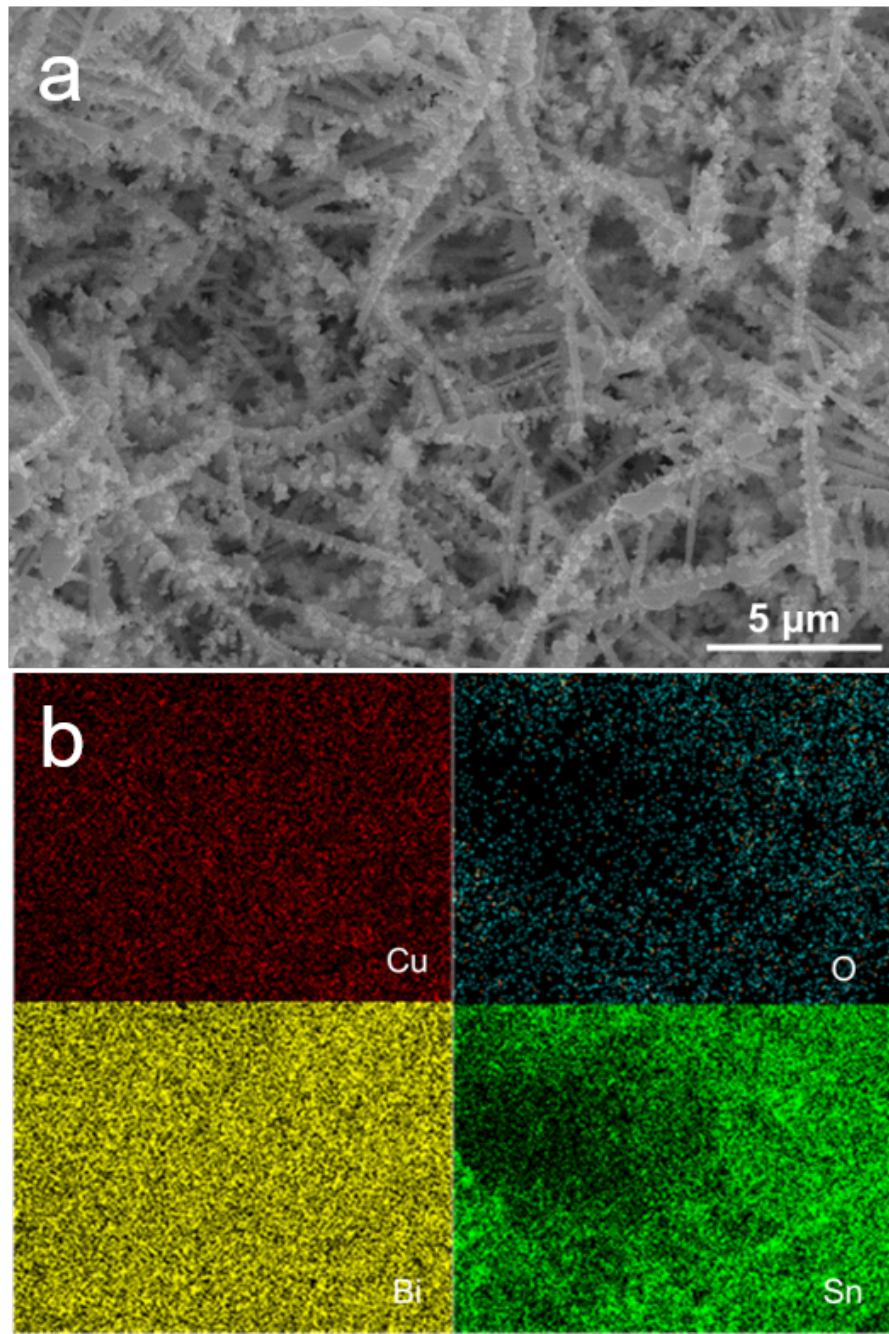


Figure S1. (a) An SEM image and (b) corresponding EDS elemental mappings of the as-synthesized dendritic BiSn sample.

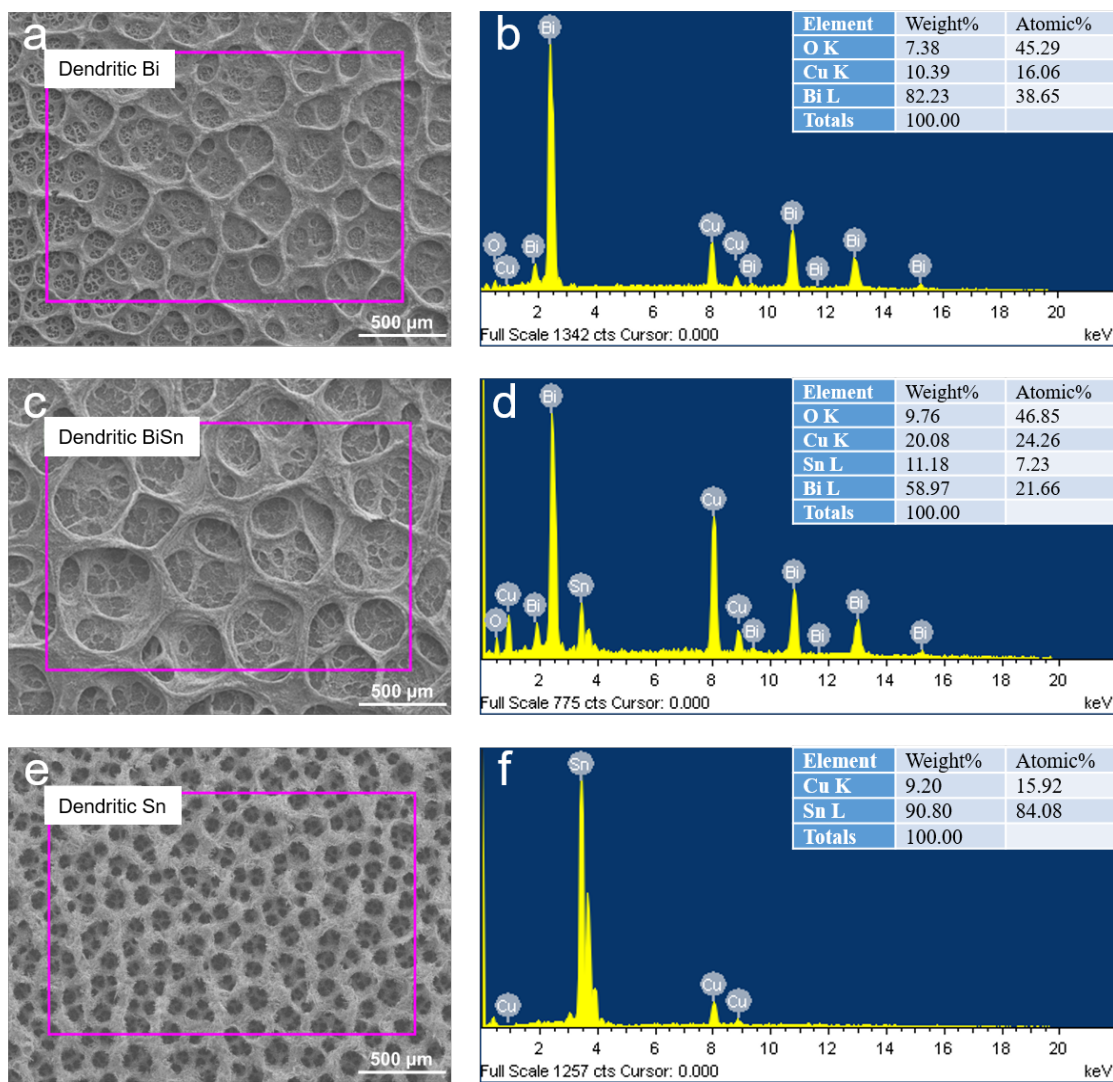


Figure S2. SEM images and corresponding EDS elemental compositions of the as-synthesized dendritic samples: (a and b) Bi, (c and d) BiSn, and (e and f) Sn

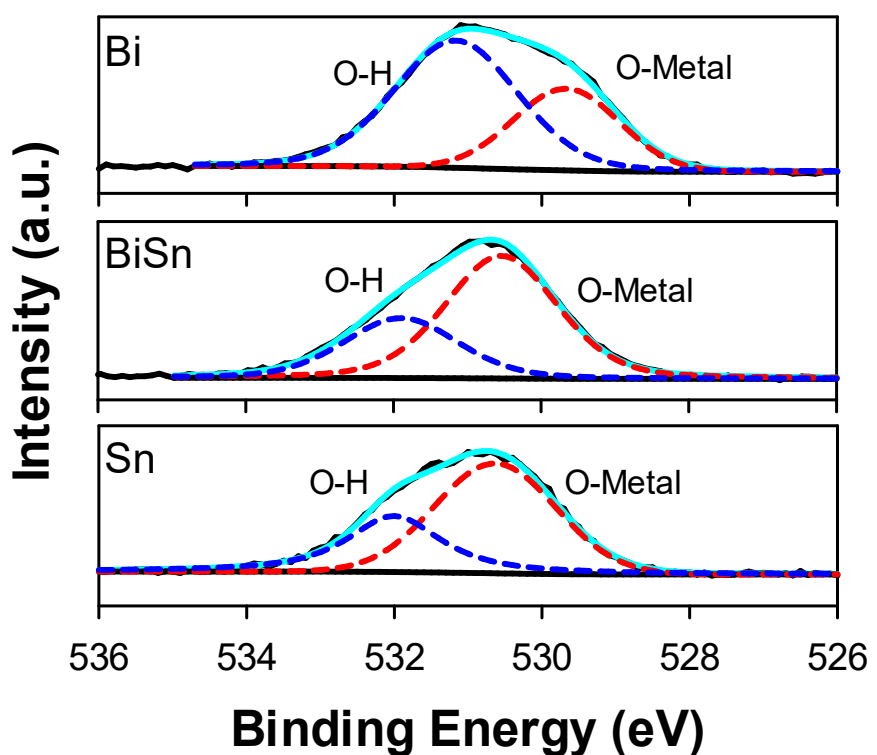


Figure S3. O_{1s} XPS spectra for Bi, BiSn, and Sn samples. The distribution patterns of the oxygen atoms coordinated to hydrogen (O-H) and metal (O-metal) were similar between the Sn and BiSn

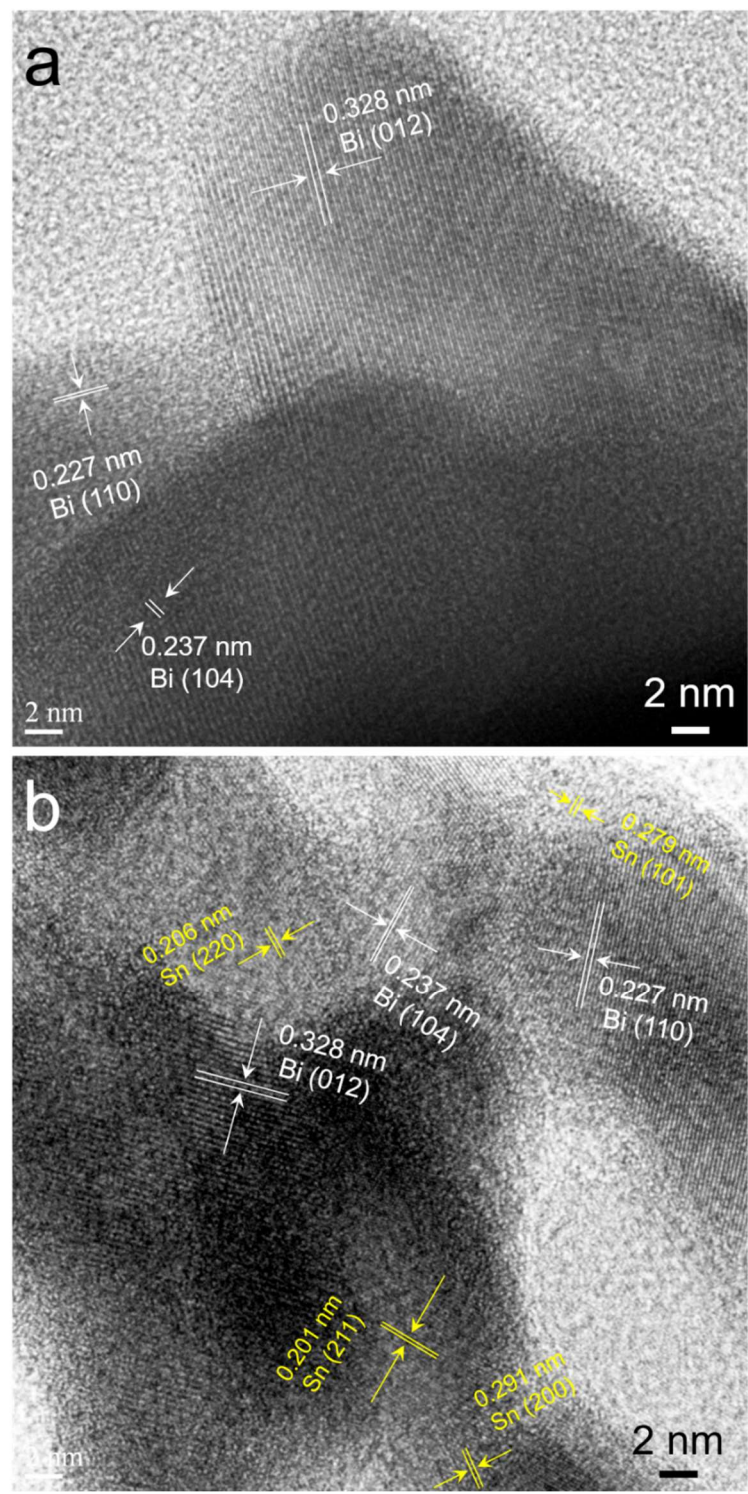


Figure S4. HR-TEM images of (a) Bi and (b) BiSn and their lattice space d values and corresponding lattice planes.

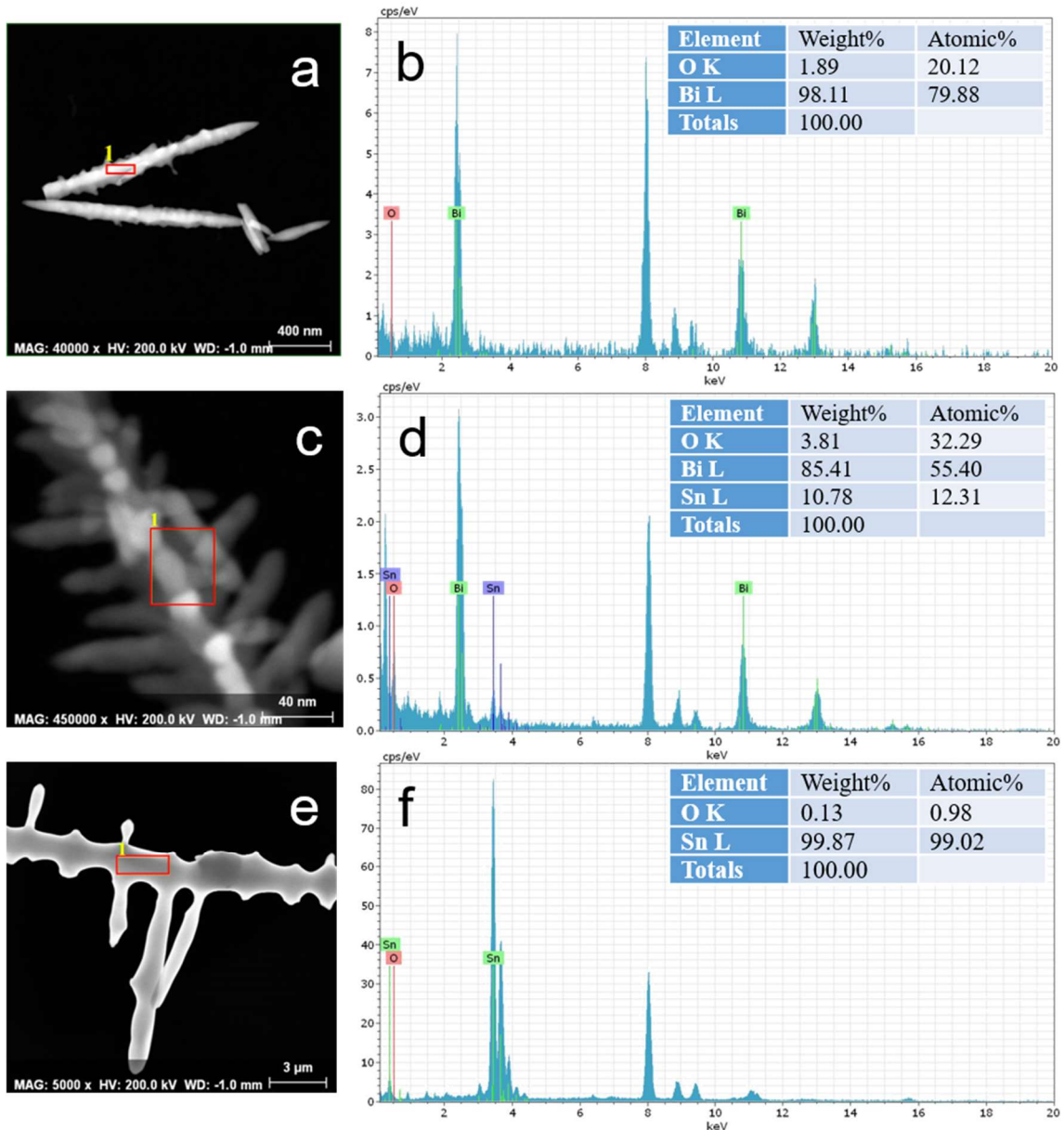


Figure S5. HAADF-STEM images and corresponding EDS elemental compositions of the as-synthesized dendritic samples: (a and b) Bi, (c and d) BiSn, and (e and f) Sn.

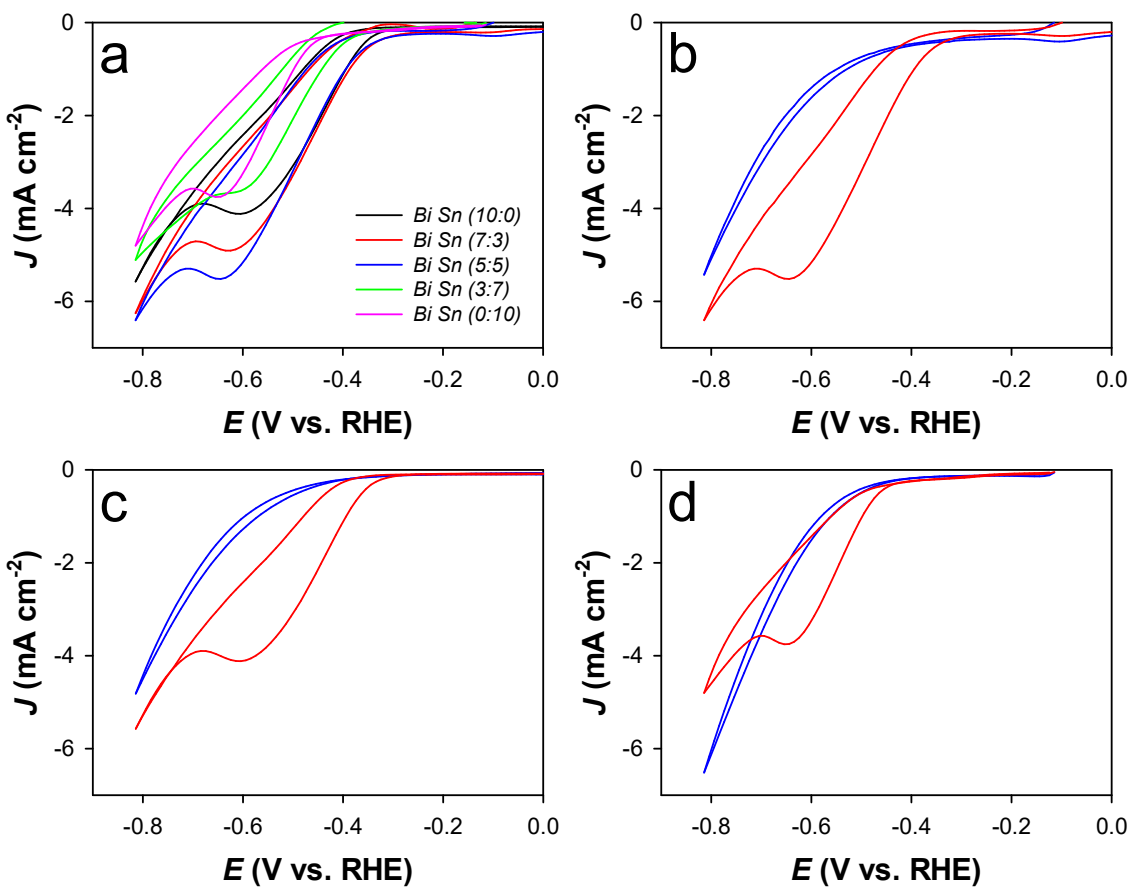


Figure S6. (a) Cyclic voltammograms of the as-synthesized dendritic BiSn electrodes as a function of Bi/Sn molar ratio in 0.5 M borate solutions (pH 9.2) containing 20 mM HMF. (b-d) Cyclic voltammograms of the as-synthesized dendritic BiSn with a Bi/Sn molar ratio of 5:5 (b), Bi (c), and Sn (d) in the borate solutions in the absence (blue) and presence (red) of HMF.

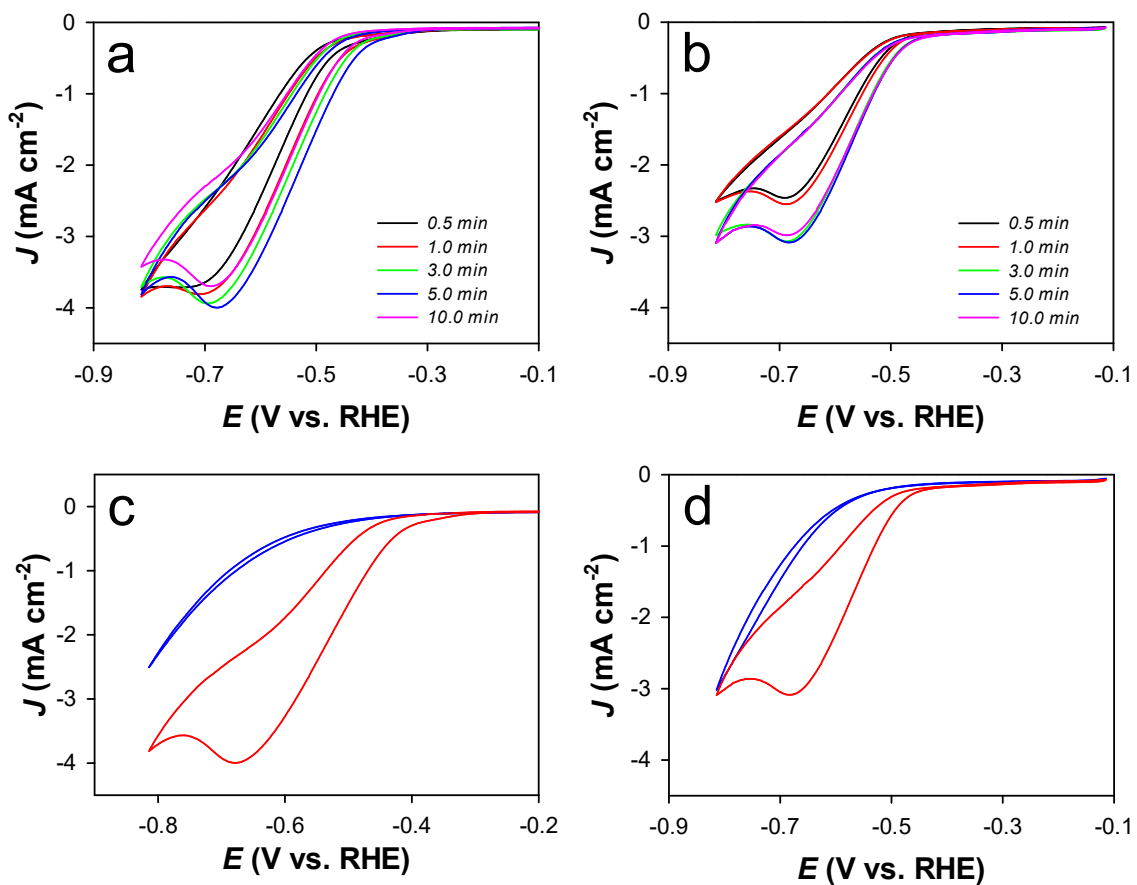


Figure S7. (a and b) Effects of electrodeposition time on cyclic voltammograms of the as-synthesized planar Bi and Sn electrodes, respectively, in 0.5 M borate solutions (pH 9.2) containing 20 mM HMF. (c and d) Cyclic voltammograms of planar Bi and Sn electrodes (with the electrodeposition time of 5 min), respectively, in the absence (blue) and presence (red) of HMF.

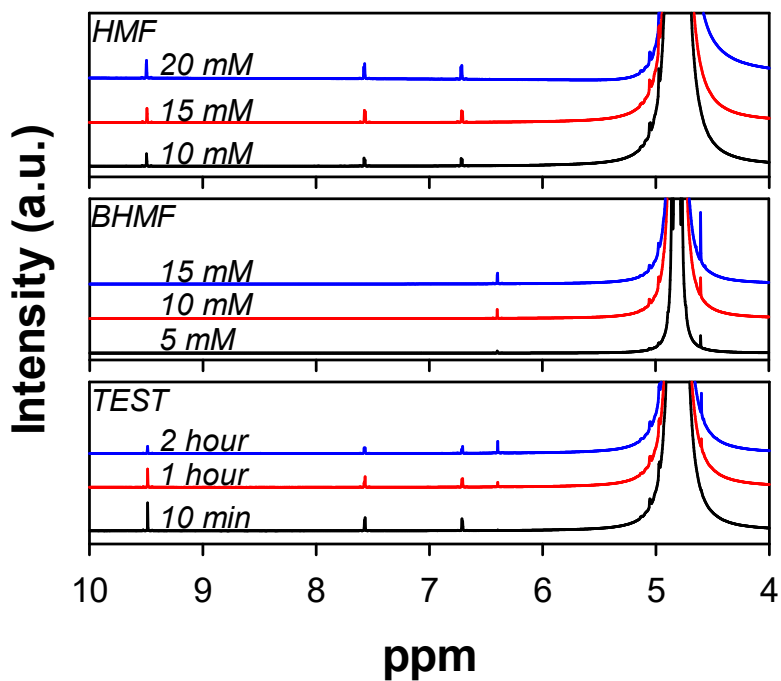


Figure S8. (Top and middle panels) ^1H -NMR spectra of standard HMF and BHMF solutions, respectively. (Bottom panel) ^1H -NMR spectra of aliquots underwent electrolysis with dendritic Bi electrode at -0.41 V vs. RHE in 0.5 M borate solution with 20 mM HMF at pH 9.2 . The NMR peaks at 9.51 , 7.57 and 6.72 ppm resulted from HMF and those at 6.40 ppm and 4.60 ppm were attributed to BHMF.

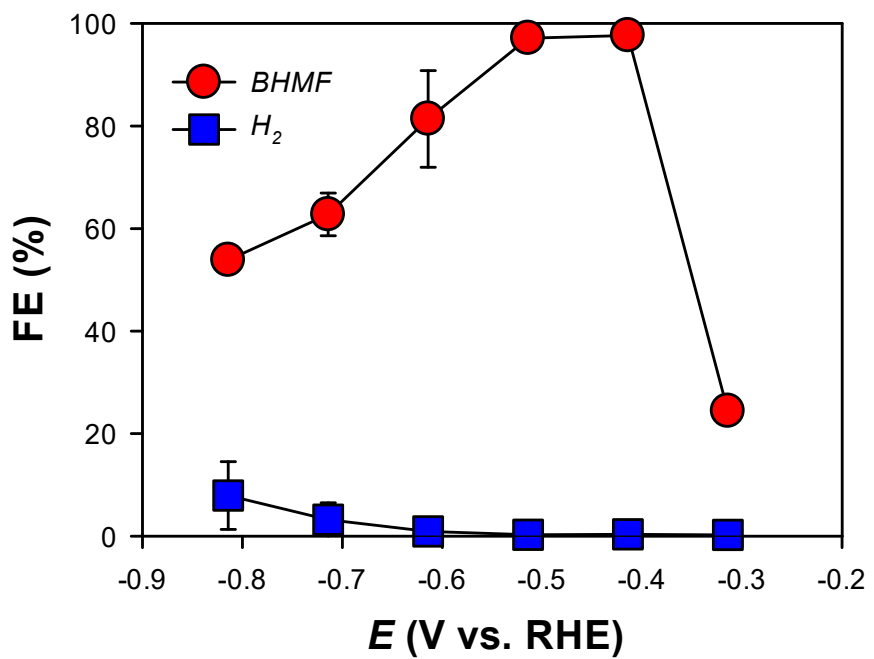


Figure S9. Effects of applied E on FEs for productions of BHMF and H₂ with dendritic Bi electrode in 0.5 M borate solutions (pH 9.2) with 20 mM HMF.

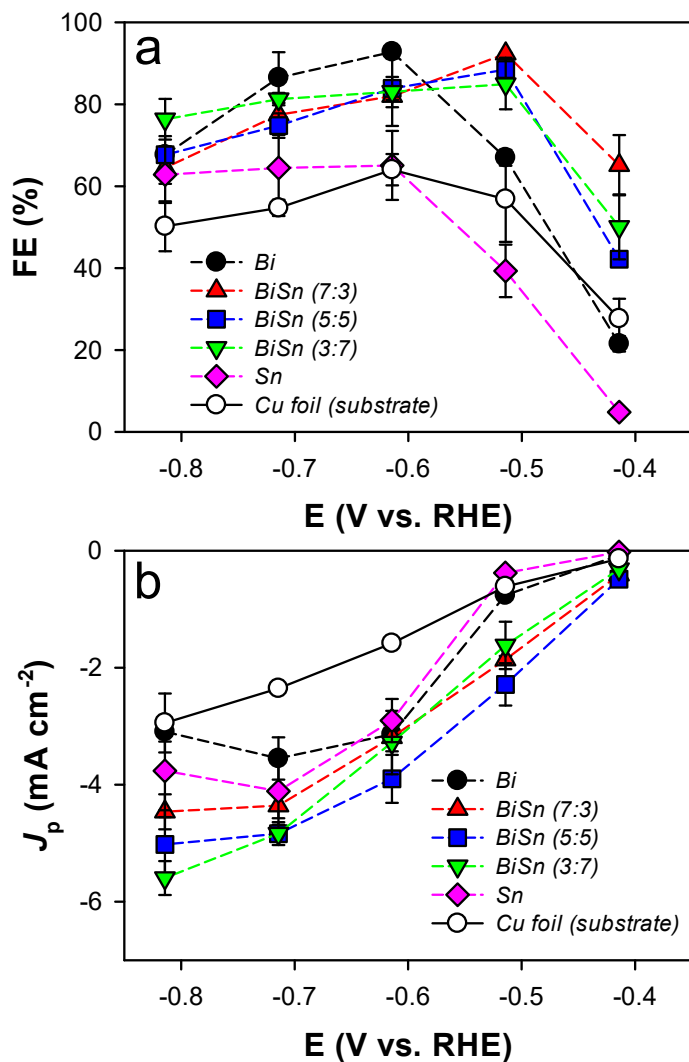


Figure S10. Electrochemical catalytic activities for HMF hydrogenation with planar electrodes (Bi, Sn, and BiSn) in 0.5 M borate solutions (pH 9.2) with 20 mM HMF. For comparison, the activity of Cu substrate was also shown. (a) FE values as a function of E . (b) Partial current density values for production of BHMF (J_p) with respect to E ($J_p = J_{ss} \times \text{FE} / 100$). All bimetallic BiSn catalysts exhibited higher FE and J_{BHMF} values than monometallic Bi and Sn. However, their activities were lower than those with dendritic BiSn (compare Figure 5a and Figure S10).

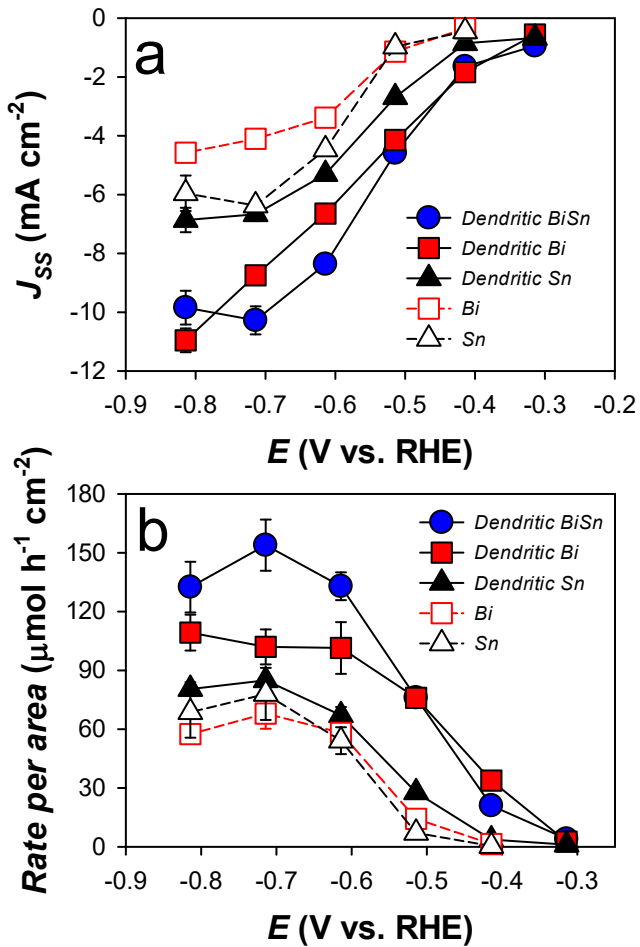


Figure S11. (a) Steady-state J (J_{ss}) values as function of E with planar and dendritic electrodes in 0.5 M borate solutions (pH 9.2) with 20 mM HMF. (b) BHMF production rate per unit area at a given E in 0.5 M borate solutions (pH 9.2) with 20 mM HMF.

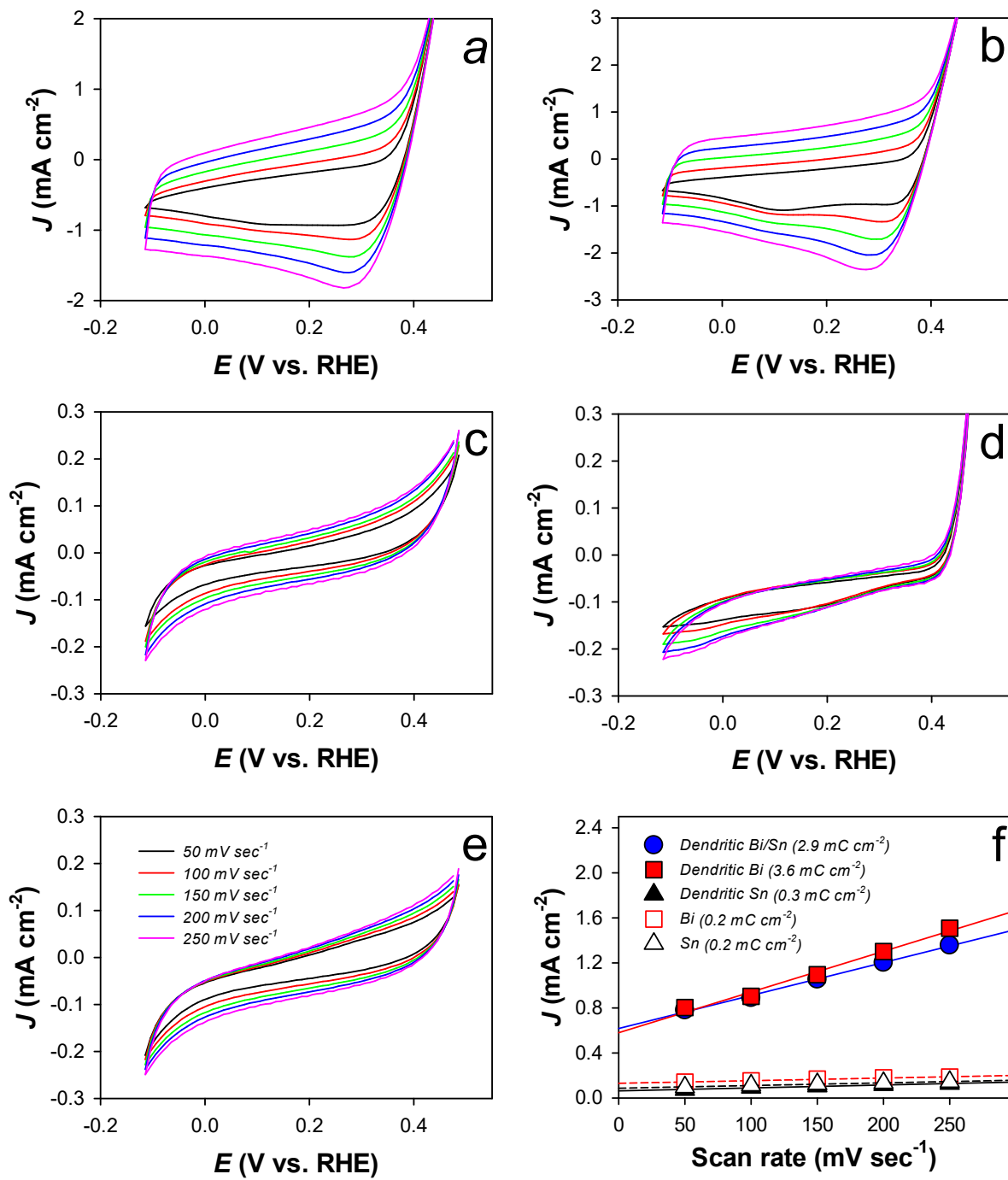


Figure S12. Cyclic voltammograms with the as-synthesized electrodes as a function of potential scan rate (50 to 250 mV s⁻¹) in 0.5 M borate solutions (pH 9.2) with 20 mM HMF. (a) dendritic Bi/Sn, (b) dendritic Bi, (c) dendritic Sn, (d) planar Bi, and (e) planar Sn electrodes. (f) Capacitive current densities (estimated at 0.1 V) as a function of scan rate. The numbers in parentheses are C_{dl} values.

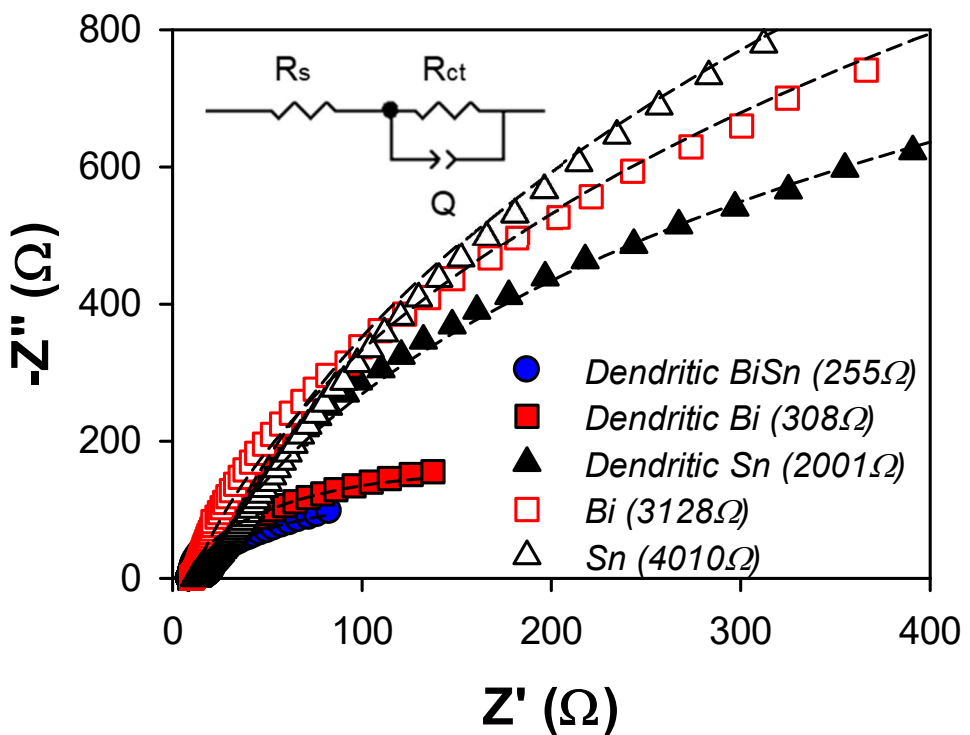


Figure S13. Nyquist plots obtained at -0.2 V vs. RHE in 0.5 M borate buffer solution (pH 9.2) with 20 mM HMF. Inset shows the equivalent circuit, where R_s , R_{ct} , and Q denote solution resistance, interfacial charge transfer resistance, and constant phase element, respectively. The numbers in parentheses are R_{ct} values.

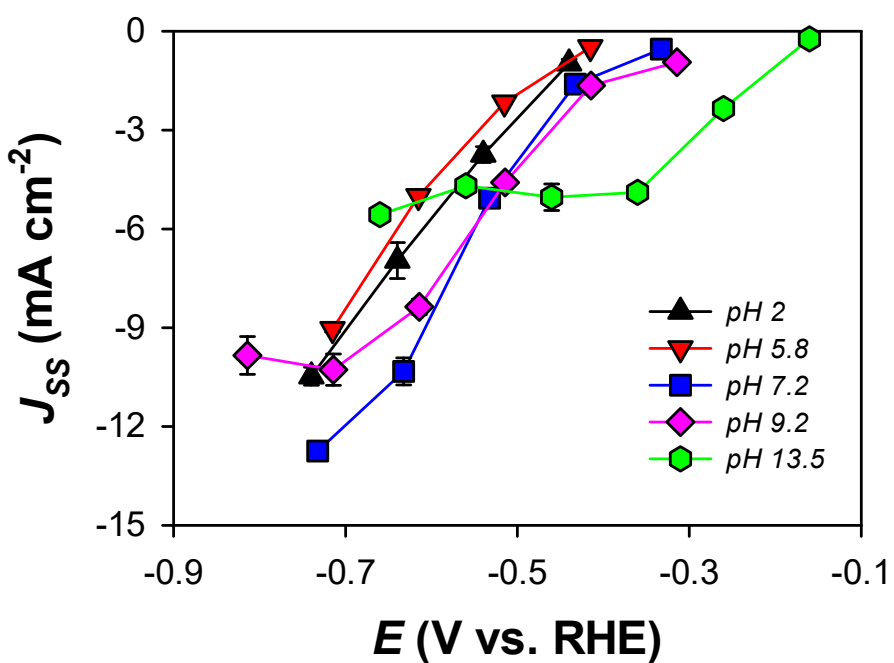
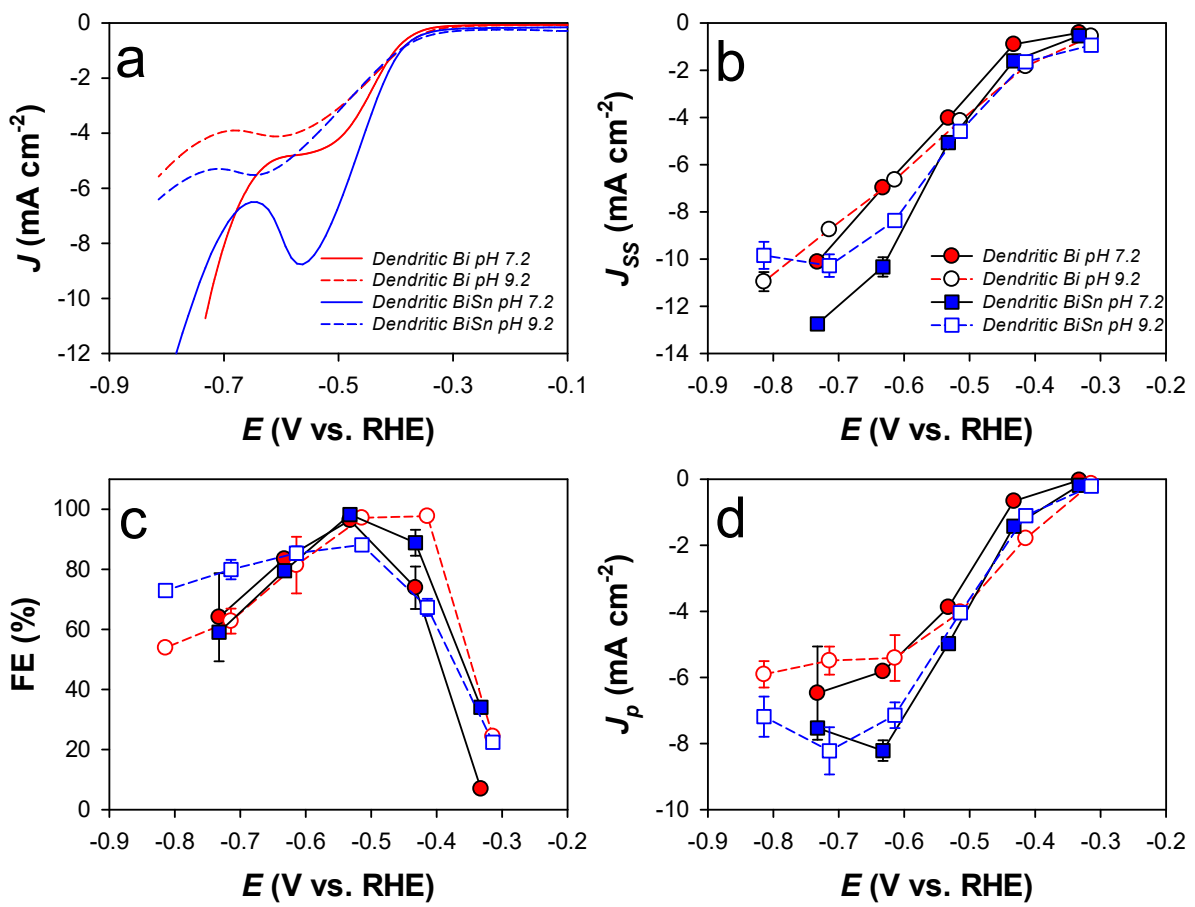


Figure S14. Effects of pH values on the J_{ss} values with as-synthesized dendritic BiSn electrodes with HMF (20 mM).



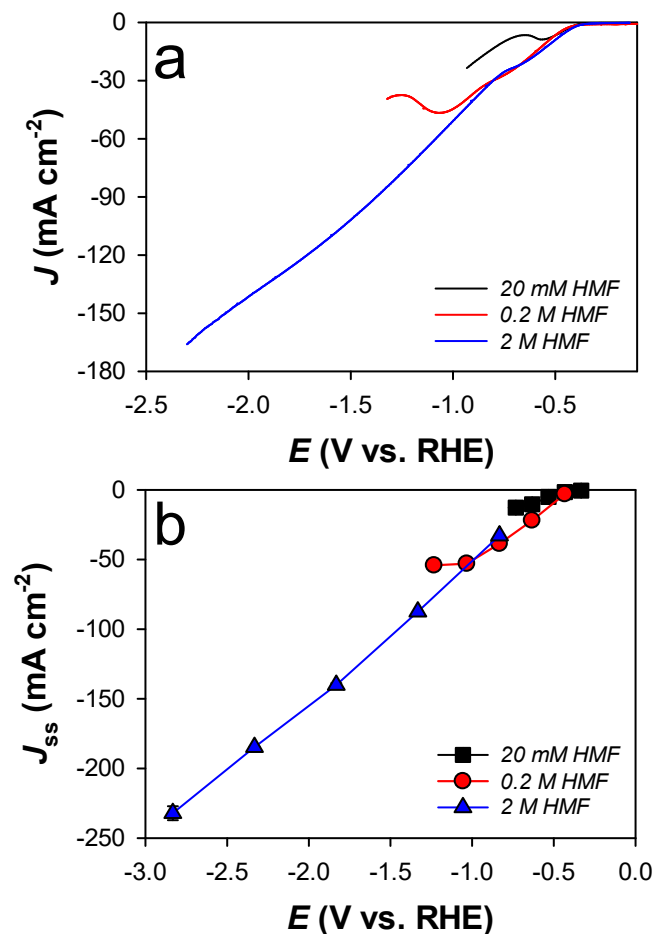


Figure S16. (a) Linear sweep voltammograms and (b) E -dependent J_{ss} with dendritic BiSn in 0.5 M phosphate buffer (pH 9.2) with various HMF concentrations.

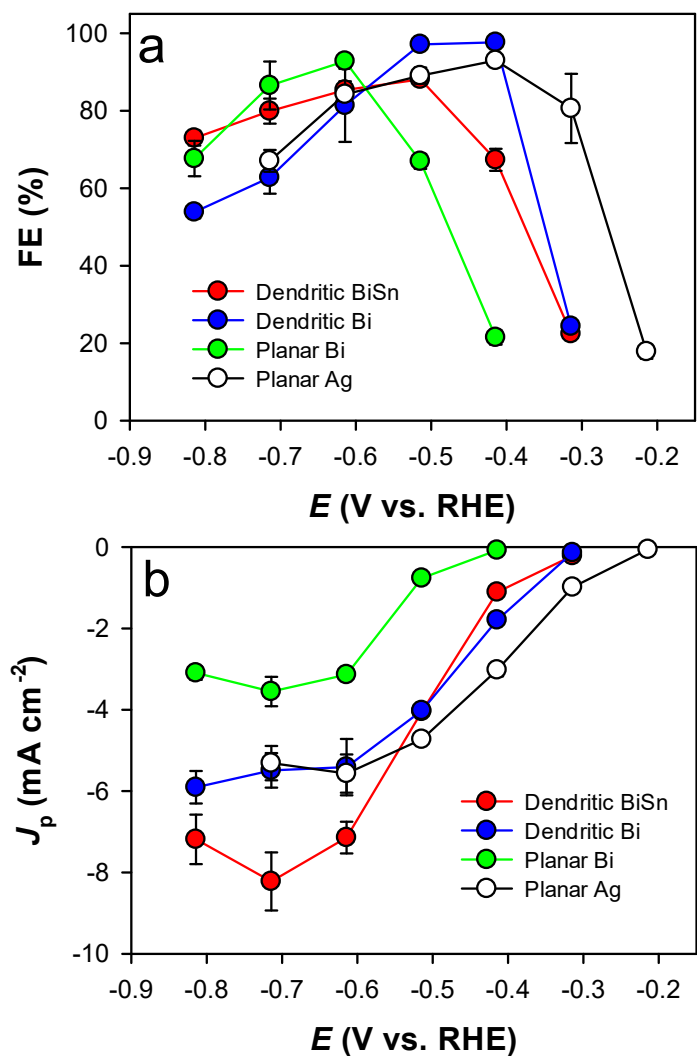


Figure S17. Comparison of electrochemical catalytic activities among Ag (planar), Bi (planar and dendritic), and BiSn (dendritic) for HMF hydrogenation in 0.5 M borate solutions (pH 9.2) with 20 mM HMF. (a) FE values as a function of E . (b) Partial current density values for production of BHMF (J_p) with respect to E ($J_p = J_{ss} \times \text{FE} / 100$).

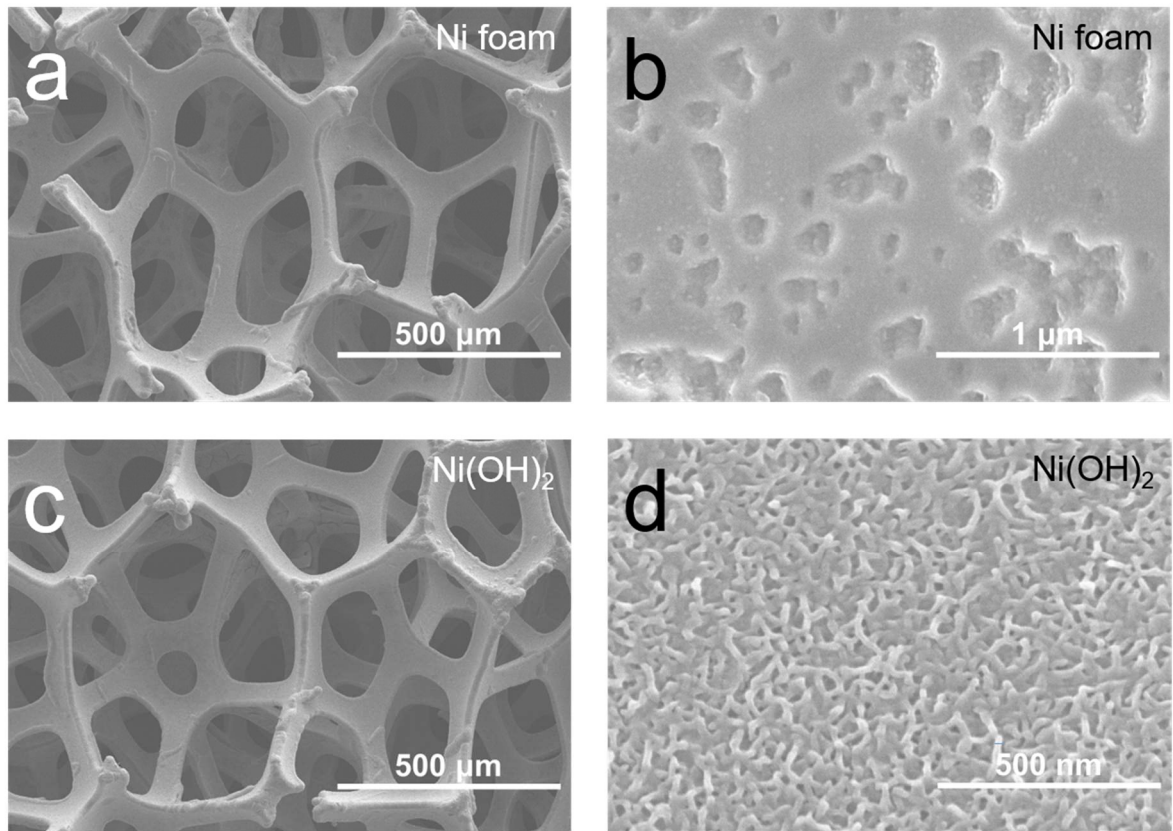


Figure S18. SEM images of (a and b) Ni foam and (c and d) Ni(OH)₂/Ni foam.

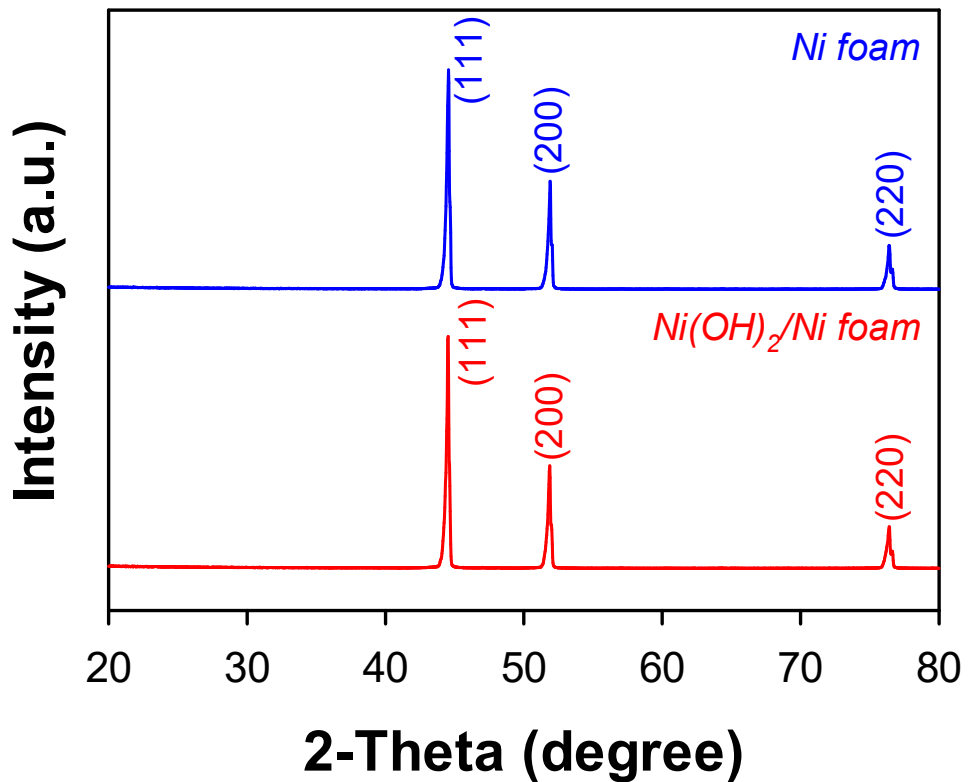


Figure S19. XRD patterns of bare and Ni(OH)₂-deposited Ni substrates (foams).

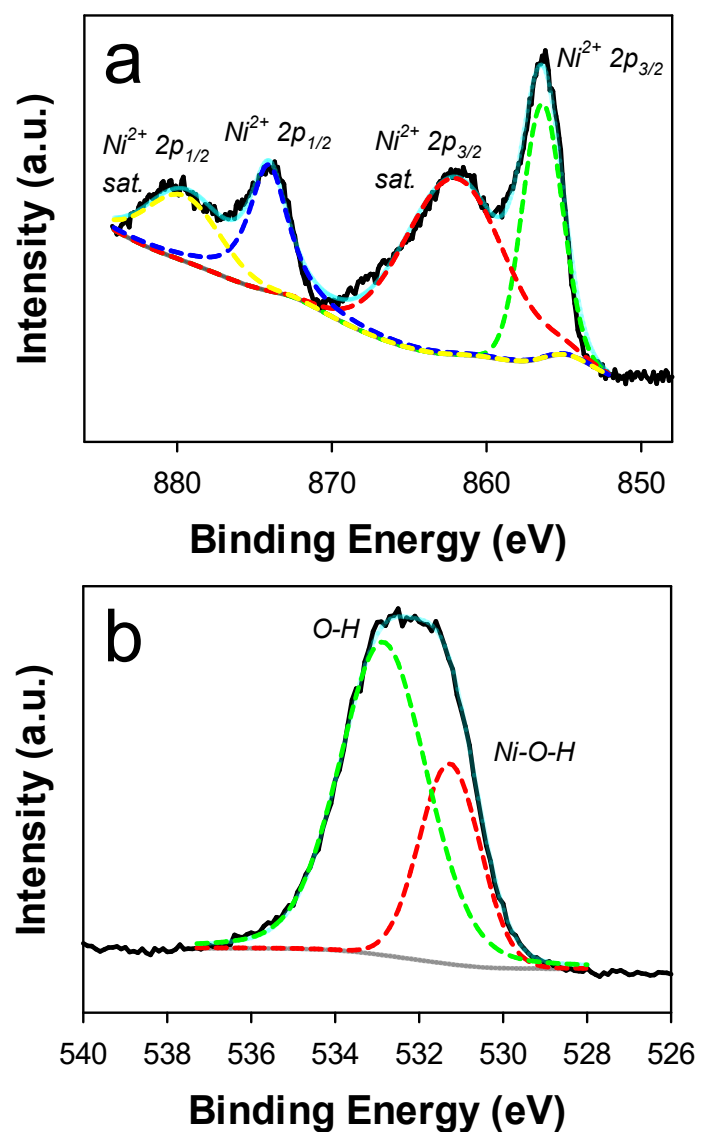


Figure S20. (a) Ni 2p and (b) O 1s XPS spectra of the as-deposited Ni(OH)_2 .

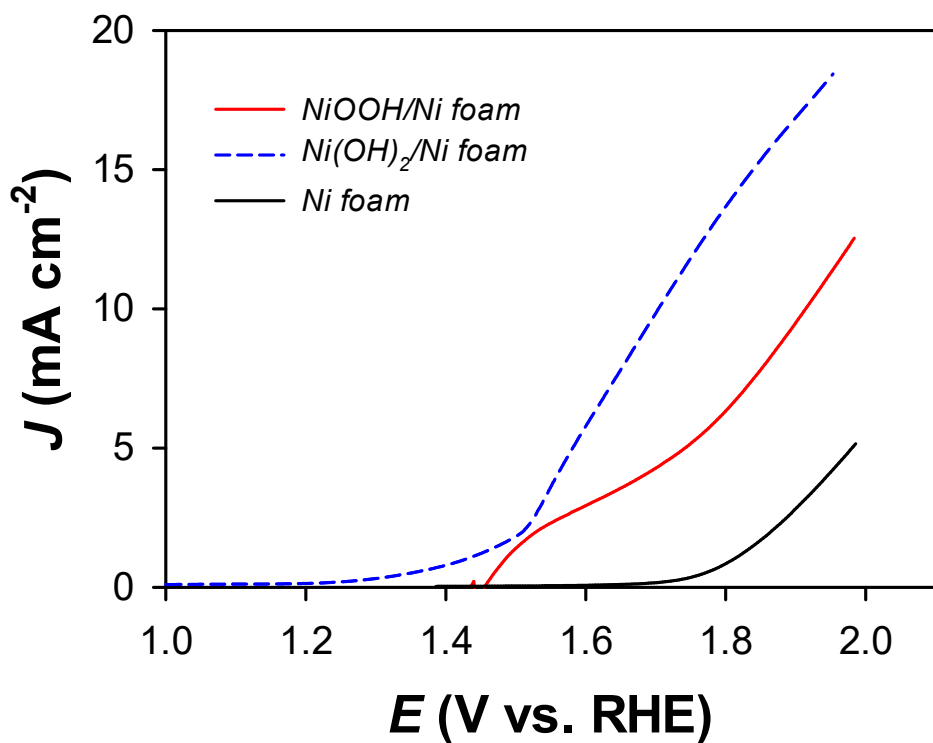


Figure S21. Linear sweep voltammograms of Ni foam (black solid), $\text{Ni(OH)}_2/\text{Ni}$ foam (blue dashed) and NiOOH/Ni foam (red solid). The NiOOH/Ni electrode was derived from the as-synthesized $\text{Ni(OH)}_2/\text{Ni}$ foam by repetitive anodic polarization.

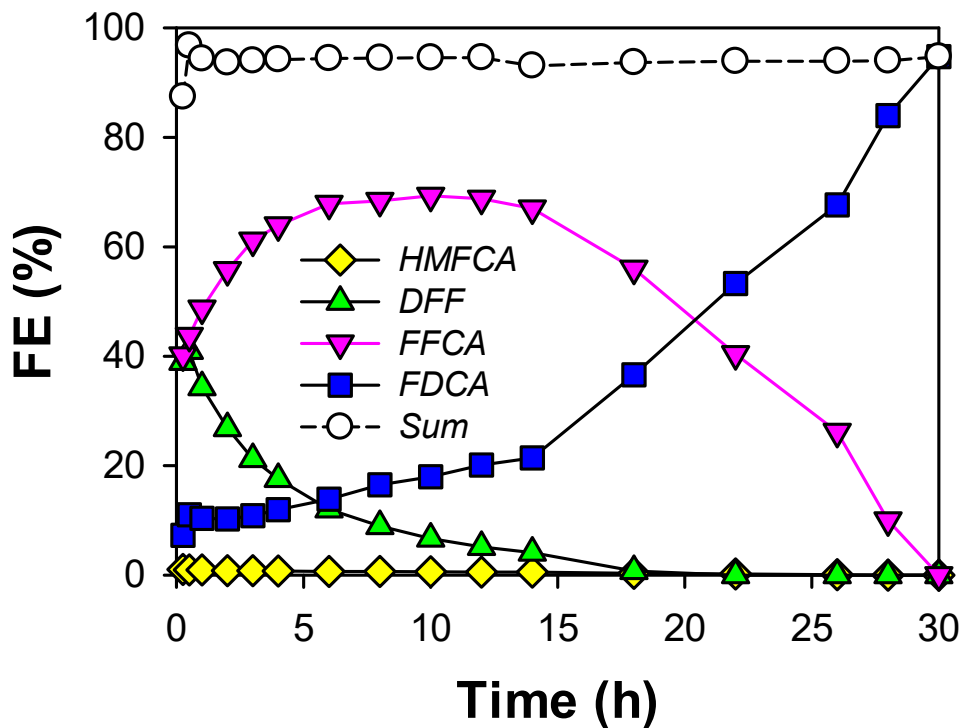


Figure S22. Time-profiled changes in FE values for productions of intermediates and FDCA during electrocatalytic oxidation of HMF with NiOOH anode in 0.5 M borate solutions with 5 mM TEMPO and 10 mM HMF at a fixed E_c of -0.53 V.